END
DATE
FILMED
9 82
DTIC

NAVAL POSTGRADUATE SCHOOL
Monterey, California

THESIS

FRICTION MEASUREMENT BY MEANS OF A GYROSCOPIC MASS

by

Thomas Leo Stowell

March 1982

Thesis Advisor: R. H. Nunn

Approved for public release; distribution unlimited.

82 08 16 157

Unclassified

REPORT DOCUMENTATION PAGE		READ INSTRUCTIONS BEFORE COMPLETING FORM
1. REPORT NUMBER	2. GOVT ACCESSION NO. AD-A118 188	3. RECIPIENT'S CATALOG NUMBER
4. TITLE (and Subtitle) Friction Measurement by Means of A Gyroscopic Mass		5. TYPE OF REPORT & PERIOD COVERED Master's Thesis March 1982
		6. PERFORMING ORG. REPORT NUMBER
7. AUTHOR(s) Thomas Leo Stowell		8. CONTRACT OR GRANT NUMBER(s)
9. PERFORMING ORGANIZATION NAME AND ADDRESS Naval Postgraduate School Monterey, California 93940		10. PROGRAM ELEMENT, PROJECT, TASK AREA & WORK UNIT NUMBERS
11. CONTROLLING OFFICE NAME AND ADDRESS Naval Postgraduate School Monterey, California 93940		12. REPORT DATE March 1982
		13. NUMBER OF PAGES 49
14. MONITORING AGENCY NAME & ADDRESS(If different from Controlling Office)		15. SECURITY CLASS. (of this report) Unclassified
		15a. DECLASSIFICATION/DOWNGRADING SCHEDULE
16. DISTRIBUTION STATEMENT (of this Report) Approved for public release; distribution unlimited.		
17. DISTRIBUTION STATEMENT (of the abstract entered in Block 20, if different from Report)		
18. SUPPLEMENTARY NOTES		
19. KEY WORDS (Continue on reverse side if necessary and identify by block number) Friction Measurement Gyroscopic Mass Coefficient of Sliding Friction		

20. ABSTRACT (Continue on reverse side if necessary and identify by block number)
Previous theoretical and experimental studies have demonstrated that when a bored sphere is contained within a spinning cavity, the sphere will rotate so that its major axis of inertia is aligned with the axis of spin of the cavity. Under certain conditions, the time required for alignment is inversely proportional to the coefficient of sliding friction. The objective of this investigation has been to investigate this phenomenon as a method for determination of the coefficient of sliding friction between various materials. An experimental

DD FORM 1473 EDITION OF 1 NOV 65 IS OBSOLETE
JAN 73
S/N 0102-014-6601

Unclassified

apparatus was designed and built and tests were conducted in order to evaluate the basic theoretical premise.

Accession For		
NTIS GRA&I	✓	
DTIC TAB		
Unannounced		
Justification		
By		
Distribution/		
Availability Codes		
	Avail and/or	
Dist	Special	
A		

DTIC
COPY
INSPECTED
2

Friction Measurement by Means of a
Gyroscopic Mass

by

Thomas Leo Stowell
Lieutenant, United States Navy
B.A., University of Minnesota, 1972
M.A., University of North Carolina, 1974

Submitted in partial fulfillment of the
requirements for the degree of

MASTER OF SCIENCE IN MECHANICAL ENGINEERING

from the

NAVAL POSTGRADUATE SCHOOL
March 1982

Author _____

Approved by: _____
                                    Thesis Advisor

_____
Chairman, Department of Mechanical Engineering

_____
Dean of Science and Engineering

3

ABSTRACT

Previous theoretical and experimental studies have demonstrated that when a bored sphere is contained within a spinning cavity, the sphere will rotate so that its major axis of inertia is aligned with the axis of spin of the cavity. Under certain conditions, the time required for alignment is inversely proportional to the coefficient of sliding friction. The objective of this investigation has been to investigate this phenomenon as a method for determination of the coefficient of sliding friction between various materials. An experimental apparatus was designed and built and tests were conducted in order to evaluate the basic theoretical premise.

4

TABLE OF CONTENTS

LIST OF FIGURES

7

NOMENCLATURE

(Only primary symbols are listed. Intermediate quantities are defined in the text.)

A   major mass moment inertia, $\text{ft} - \text{lb} - \text{sec}^2$

C   minor mass moment inertia, $\text{ft} - \text{lb} - \text{sec}^2$

D step input of linear approximation

M   magnitude of applied torque, $\text{ft} - \text{lb}$

r   radius of concentric hole, in

$\hat{r}$ ratio of r to R

R   radius of ball, in

$\mathcal{R}$ ramp input of linear approximation

W   weight of ball, lb

ζ damping factor

θ angle between concentric hole and axis of rotation, radians

λ $\dfrac{C-A}{A}$

μ_s coefficient of sliding friction

ω_o spin rate of cylinder, sec^{-1}

8

ACKNOWLEDGMENTS

I. INTRODUCTION

A. BACKGROUND

1. History

The motivation for this thesis study is derived from previous investigations of a unique method for the sealing (obturation) of tubular projectiles. For this reason, a brief review of this previous work is presented here.

For over 100 years, a significant amount of research has ꞏ ꞏ devoted to investigating the advantages and disadvantages of tubu projectiles. For the most part, tests indicate that tubular pro: 'es have 1/3 to 1/2 the drag of conventional projectiles. The low dr ʋ of the tubular projectile implies that it can be fired at flatter trajectories and will reach its target quicker. Until recently, tubular projectiles have utilized sabots or pushers which were discarded upon firing. The possibility of ingestion of these sabots into the engines of launch aircraft has prohibited the use of tubular projectiles in this application.

A recent development by the Naval Weapons Center, China Lake, CA. has been the Ball-Obturated Tubular (BOT) Projectile (Fig. 1). The basic idea behind this design is that a spinning mass will tend to spin about its major axis of inertia. The ball-obturator is bored with a concentric hole the same diameter as the hole through the projectile. When loaded, the ball is positioned inside the projectile so that the axis of its hole is nearly perpendicular to the axis of the projectile.

10
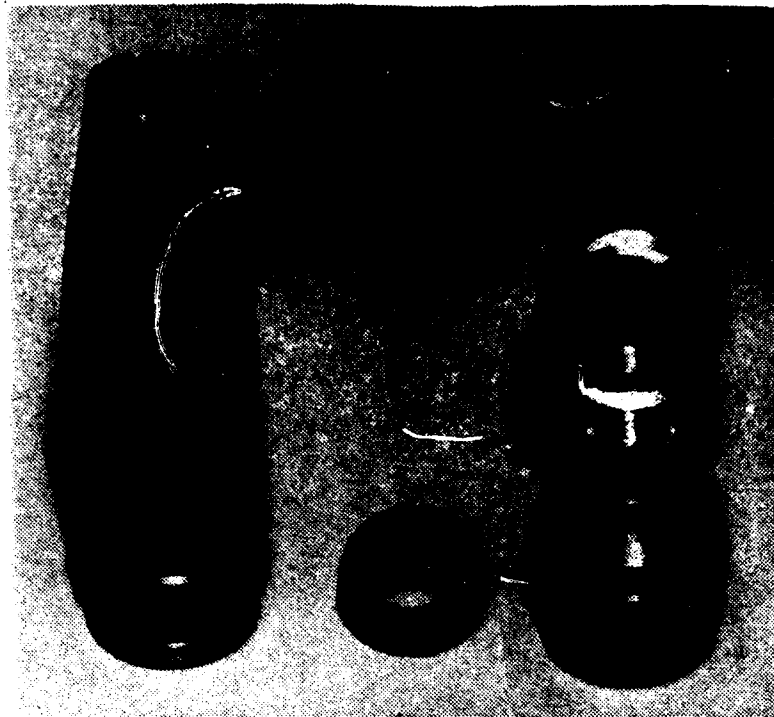
Figure 1: 20mm Ball-Obturated Tubular Projectile [1]

Gas pressure from the burning propellant holds the ball-obturator fixed
with respect to the projectile. Upon exiting the gun barrel, the pro-
pellant gas pressure is released and aerodynamic forces come int. play.
A complex force distribution acts on the ball causing it to nutate in-
side the projectile to decrease its inertial imbalance. The ball will
continue to nutate until its major axis of inertia (axis of the concen-
tric hole) is aligned with the hole in the projectile. Inertial forces
will then dominate to maintain this alignment. It is to be noted that
the opening process is automatic and that there are no discarded parts.

11

2. Theoretical Model of BOT

Nunn and Bloomer [1,2] developed a theoretical model to predict the motion of the ball-obturator as a function of time. Computer solutions, henceforth referred to as "exact" solutions, indicate that the ball motion at high projectile spin rates can be approximated by a linear damped system with step and ramp inputs (Fig. 2).
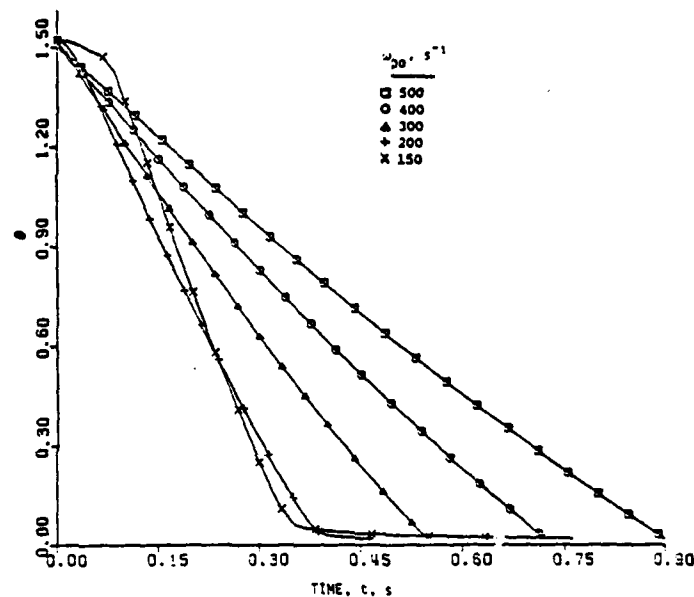
Figure 2:   Exact Solutions for Ball Tilt Angle θ v.s. Time [1]

A comparison between the linear approximation and the exact solution for an initial angle, θ_0, with the ball resting against the cavity under a gravity load, shows good agreement during the initial phase of motion (Fig. 3).   Experiments conducted by Nunn and Bloomer verify the form of their linear approximation.   At high spin rates, the elapsed time, t^*, for a given amount of nutation varies directly with the spin rate, ω_0, i.e., $t^* = k\omega_0$.   Since the constant of proportionality,

12

k, involves the coefficient of sliding friction, μ_s, it appears that their experimental method can alternatively be used as a scheme for measuring μ_s, that is, with k determined from the theory or through calibration a knowledge of ω_0 and t* provides a means of determining μ_s.
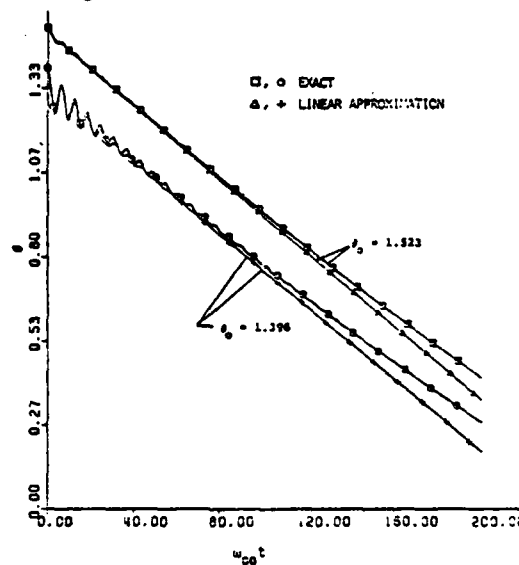
Figure 3: Comparison of Approximate Solutions with Exact Solutions. Gravity Load Only, Ball MOD 0, ω_{po}=400 sec^{-1} [1]

It is this observation that has led to the definition of the goals of this study. Before describing these goals, however, a brief review will be given of the original experimental apparatus along with some other methods that have been used for measuring sliding friction.

3. Experimental Apparatus for BOT

The experimental apparatus used in the projectile study was designed and built to simulate the BOT under the influence of a gravity load (Fig. 4). A 5/8 inch steel ball with a concentric hole was fitted into a spherical cavity machined into a cylindrical plexiglas housing. The cylinder rotated on ball bearings mounted in aluminum pillow blocks

13

on a rigid pedestal. One end of the cylinder was press-fit into a tur-
bine wheel that was driven by an air jet to achieve a desired speed of
rotation.
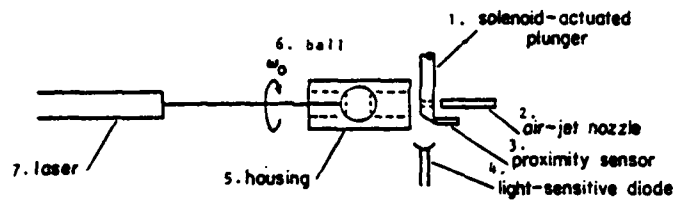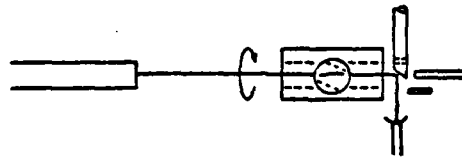
(a) Initial position with $\theta=\theta_0$, laser beam blocked.

(b) Final position with $\theta=\theta^*$, laser beam transmitted and reflected
to light-sensitive diode [2].

Figure 4: Sketch Illustrating Method for Sensing t*

In its initial position, the ball was set so that its hole was
nearly perpendicular to the cylinder axis. This obstructed a laser
beam which was aligned with the axis of rotation (the cylinder axis).
The ball was held in place within the cavity by a jet of compressed air
while the cylinder was brought up to a designated speed of rotation.
After this speed was achieved, a solenoid-actuated plunger was re-
tracted. This action started an electric timer and blocked the holding
jet (the jet was also simultaneously switched off by a fast acting
solenoid) allowing the ball to move more freely relative to the cylinder.

14

The ball would then nutate to reduce the inertial imbalance which existed because its major axis of inertia (the hole axis) was not in alignment with the axis of rotation. After the ball nutated through a large enough angle, the laser beam became unobstructed, passed through the cylinder, and reflected off the beveled and polished end of the plunger into a light-sensitive diode stopping the electric timer and signaling the end of the event.

B. OTHER EXPERIMENTAL TECHNIQUES

1. Typical Friction Apparatus

A typical mechanical apparatus used to measure friction is shown schematically in Fig. 5 [4]. Friction is measured between a flat sliding lower surface and a stationary upper surface called a rider. Movement of the lower surface sets up a frictional force between the two surfaces and the amount of deflection of the rider is proportional to that force. This apparatus normally operates at high loads and low sliding speeds. For high speeds, similar arrangements are often used except the rider is pressed against the rim of a revolving disk instead of a flat plate. Difficulties with these types of apparatuses generally involve mechanical vibrations and severe frictional heating.
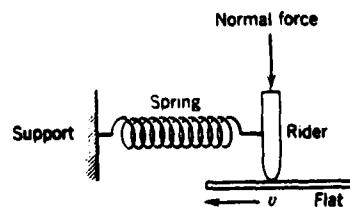
Figure 5: Representation of a Typical Frictional Apparatus [4]

15

2. High Speed Frictional Apparatus

A radical departure in experimental techniques, based on the friction-driven continuous deceleration of a rapidly rotating sphere, was conducted by Bowden and Freitag in 1958 [5]. Figure 6 represents the apparatus used in their experiments. A steel ball was suspended in the magnetic field of a solenoid, with vertical stability maintained by means of a photoelectric feedback system. The freely-suspended ball was then accelerated by a rotating magnetic field of constant frequency in a low pressure atmosphere. The ball was arranged to spin very close to three flat pads mounted symmetrically, 120 degrees to each other. The
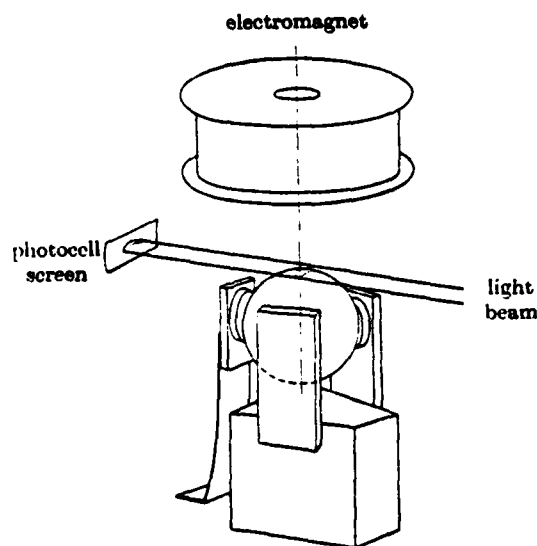
Figure 6: Schematic Diagram of High-speed Friction
Apparatus Showing Magnetic Suspension of
Steel Ball between Three Symmetrically
Placed Friction Pads [5]

three surfaces were then brought into contact with the ball causing it to slow down. The rotational deceleration, $\dot{\omega}$, provided a means of calculating the coefficient of sliding friction since:

$$\mu_s = \frac{F}{N} = \frac{I\dot{\omega}}{3RN}$$

where F = friction force

N = normal force

I = moment of inertia of the ball

R = radius of the ball

An obvious and severe limitation of this apparatus is that useful experimentation is restricted to measurements between material combinations in which at least one material is magnetic.

3. Discussion of Experimental Techniques

These existing experimental techniques involve careful control of motion and the precise measurement of pertinent forces. The apparatuses are characteristically complex and, because of difficulties in obtaining precise motion control and force or torque measurements while in operation, they are subject to inaccuracies. The apparatus of Nunn and Bloomer, however, is of simple construction and requires only the measurement of angular distance traversed and the time elapsed for this increment of motion. Furthermore, their procedures allow a wider freedom in the selection of materials, speed of relative motion, surface finishes and operating conditions such as temperature and lubrication of the surfaces.

C. PURPOSE OF STUDY

As mentioned previously, the existence of a t^* vs. ω_0 proportionality at high spin rates leads one to expect that experimental measurement of t^* and ω_0, for large ω_0, provides a method for determining the coefficient of sliding friction. The purpose of this study has been to determine the feasibility of using the linear approximation as the basis of an experimental method for the determination of the coefficient of sliding friction.

17

II. THEORETICAL BASIS AND EXPERIMENTAL METHOD

A. THEORETICAL BASIS

As previously mentioned, the theoretical results in Fig. 2 can be approximated by a second-order linear system with a ramp and step input. Specifically [1]:

$$\theta = \theta_0 + D + R(\omega_0 t - 2\zeta) \tag{1}$$

$$+ \exp(-\zeta\omega_0 t) \left\{ R\sin\left[(1-\zeta^2)^{\frac{1}{2}}\omega_0 t + \emptyset_R\right] \right.$$

$$\left. + D\sin\left[(1-\zeta^2)^{\frac{1}{2}}\omega_0 t + \emptyset_D\right] \right\} / (1-\zeta^2)^{\frac{1}{2}}$$

where θ = angle of tilt of the ball hole axis measured from the cavity
spin axis

θ_0 = initial value of θ

$\dfrac{\emptyset_R}{2} = \emptyset_D = \tan^{-1}\left[(1-\zeta^2)^{\frac{1}{2}}/\zeta\right]$

The parameters are:

$$\zeta = \frac{M}{2} \quad \text{(damping factor)} \tag{2}$$

$$D = -\frac{\lambda}{2}\sin 2\theta_0 \quad \text{(step input)} \tag{3}$$

$$R = \frac{MD}{\lambda + 1} \quad \text{(ramp input)} \tag{4}$$

where the quantity M is the non-dimensional form of the applied torque due to sliding friction between the ball and the spinning cavity. The expression for M is:

18

$$M = \frac{2\mu_s \ WR \ (\lambda+1) \ E \ (\theta_0)}{\pi\lambda A \ \omega_0^2 \ \cos \ \theta_0}$$

where $E(\theta_0)$ is the Complete Elliptic Integral of the second kind with modular angle θ_0. Under the constraints of the linearization, the validity of the approximation requires that $M \ll 1$.

When the quantity $\zeta\omega_0 t$ is sufficiently large, the oscillatory portion of the motion described by Eq. (1) may be neglected. Under this condition, Eq. (1) may be rewritten as follows:

$$\theta = \theta_0 + \mathcal{D} + \mathcal{R}(\omega_0 t - 2\zeta) \tag{6}$$

Combining Eqs. (2)-(6) and solving for t yields:

$$t = \frac{\pi A \omega_0 \left[(\theta_0-\theta)-\frac{\lambda}{2} \ \sin \ 2\theta_0\right]}{2\mu_s \ WR \ \sin \ \theta_0 \ E(\theta_0)} + \frac{2\zeta}{\omega_0} \tag{7}$$

the quantity t represents the elapsed time during an excursion from θ_0 to θ. For cases in which ω_0 is large, this becomes:

$$t = \frac{\pi A \left[(\theta_0-\theta)-\frac{\lambda}{2} \ \sin \ 2\theta_0\right]}{2\mu_s \ WR \ \sin \ \theta_0 \ E(\theta_0)} \ \omega_0 \tag{8}$$

Equation (8) illustrates the proportionality between elapsed time and spin rate for a given angular excursion $(\theta_0-\theta)$ at high values of ω_0. Nunn [3] also developed a rationale for estimating conditions necessary to avoid a hovering motion of the ball near its initial orientation. Such motion is illustrated in Fig. 2 at the lowest spin rate (150 rad/sec). In particular, hovering of the ball occurs when

$$\frac{M}{(\lambda+1)\sin \ \theta_0} \leq 1$$

19

This means that to avoid hovering:

$$\omega_0 \geq \left[\frac{4\mu_s \; WRE \; (\theta_0)}{\pi A \lambda \; \sin 2 \; \theta_0}\right]^{\frac{1}{2}} \tag{9}$$

Equation (9) ensures a rapid departure of the ball from its initial angle θ_0. Recalling again that Eq. (1) is subject to the constraint $M \ll 1$ implies that:

$$\omega_0 \gg \left[\frac{2\mu_s \; WR \; (\lambda+1) \; E \; (\theta_0)}{\pi\lambda A \; \cos \; \theta_0}\right]^{\frac{1}{2}} \tag{10}$$

Of the constraints given by Eqs. (9) and (10), the quantity given in Eq. (10) has the largest values for typical designs and therefore represents the minimum acceptable value for ω_0. In practice, the highest possible values of ω_0 should be used when deducing the coefficient of friction from Eq. (8). In addition, since Eq. (6) is only valid if $\zeta\omega_0 t$ is sufficiently large, oscillatory motion will be avoided if:

$$t \gg \frac{\pi\lambda A \; \cos \; \theta_0 \; \omega_0}{\mu_s \; WR \; (\lambda+1) \; E \; (\theta_0)} \tag{11}$$

Equation (11) may also be thought of as an effective upper bound of the spin rate ω_0.

Equation (8) may be rewritten in the form:

$$t = T \; \omega_0$$

where
$$T = \frac{\pi A \left[(\theta_0-\theta)-\frac{\lambda}{2} \sin 2 \; \theta_0\right]}{2\mu_s \; WR \; \sin \; \theta_0 \; E \; (\theta_0)}$$

20

Therefore, if a given ball, with the parameters A, λ, W, and R known, is allowed to rotate from a fixed angle, θ_0, thru a set increment, $\theta_0-\theta$, at various cavity spin rates, ω_0, then the measurements of the elapsed time t as a function of ω_0 leads to an experimental evaluation of T. This value of T will in turn lead to the determination of the coefficient of sliding friction, μ_s.

B. EXPERIMENTAL METHOD

1. Air-jet Holding Device

An elapsed time of particular interest is that required for an unobstructed path down the centerline of the spinning cavity to first occur. The angle, $\theta*$, associated with this time, t*, is illustrated in Fig. 7 and given by

$$\theta* = \sin^{-1} \left(\frac{r}{R}\right) = \sin^{-1} (\hat{r})$$

and is a design variable for the experimental apparatus. The occurrence of the angle $\theta*$ is especially suited to optical methods and it is this circumstance, in conjunction with the intention of simulating the BOT, that led to the previous experimental techniques [1].

To increase the versatility of the experimental apparatus, and in an attempt to reduce the scatter of data, several design changes were made. First, the diameter of the ball was increased to 15/16 inch to increase the mass moment of inertia about the minor axis, A, thereby reducing the spin rate required to avoid hovering. This was thought to be necessary because of earlier difficulties in holding the ball in position at high spin rates [1]. Secondly, the spherical cavity was changed to the configuration shown in Fig. (7). This configuration

provides a better seating for the ball when under the influence of the
holding jet. It also allows simple tubular inserts to be fitted into
the cavity to permit the measurement of the coefficient of friction for
different materials without major alterations to the equipment.
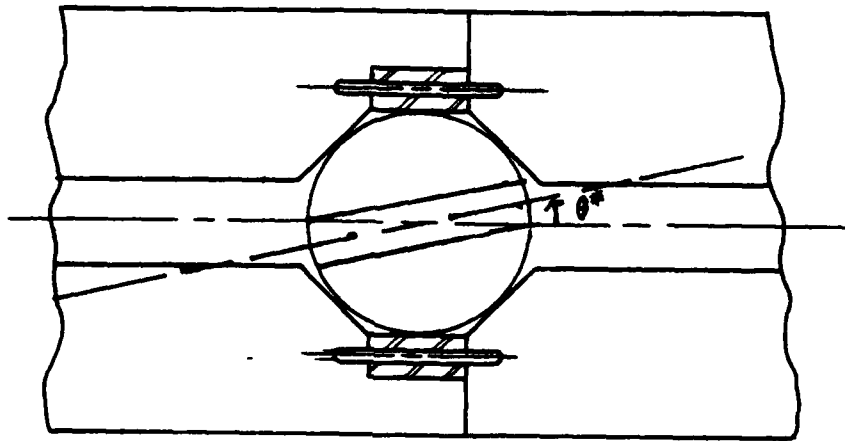
Figure 7: Diagram of Ball Cavity Showing Steel
Tubular Insert and Ball Tilt Angle at
Time t*

Thirdly, a hole passing through the center of the cavity and having the
same diameter as the concentric hole in the ball was bored through the
cylinder at an angle θ_0 to the cylinder axis. This provided a simpler
and more positive method of establishing the initial position of the
ball, see Fig. (8). Finally, because of difficulties in maintaining a
specific spin rate, particularly when the solenoid-actuated plunger was
retracted (obstructing and simultaneously switching off the holding jet),
the air-driven turbine was replaced by an electric motor with a flexible
coupling as a means of driving the rig. Figures (9) and (10) illustrate
the main elements of the apparatus.
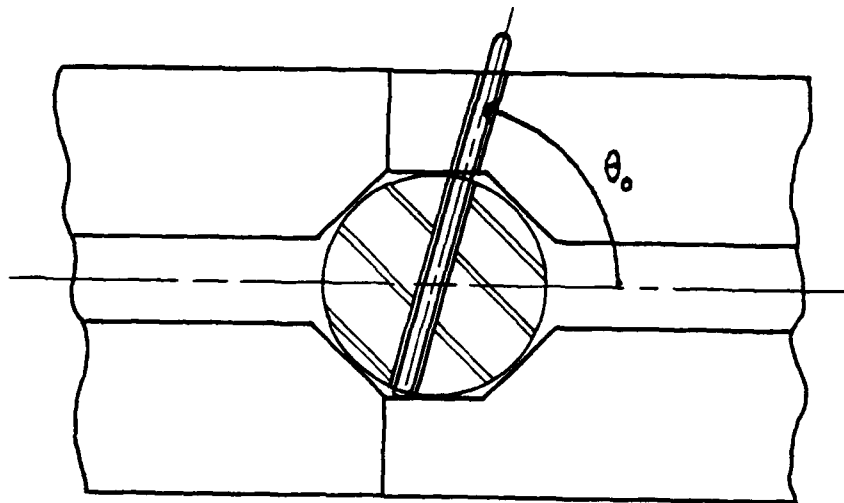
Figure 8: Diagram Illustrating Establishment
of Initial Ball Position
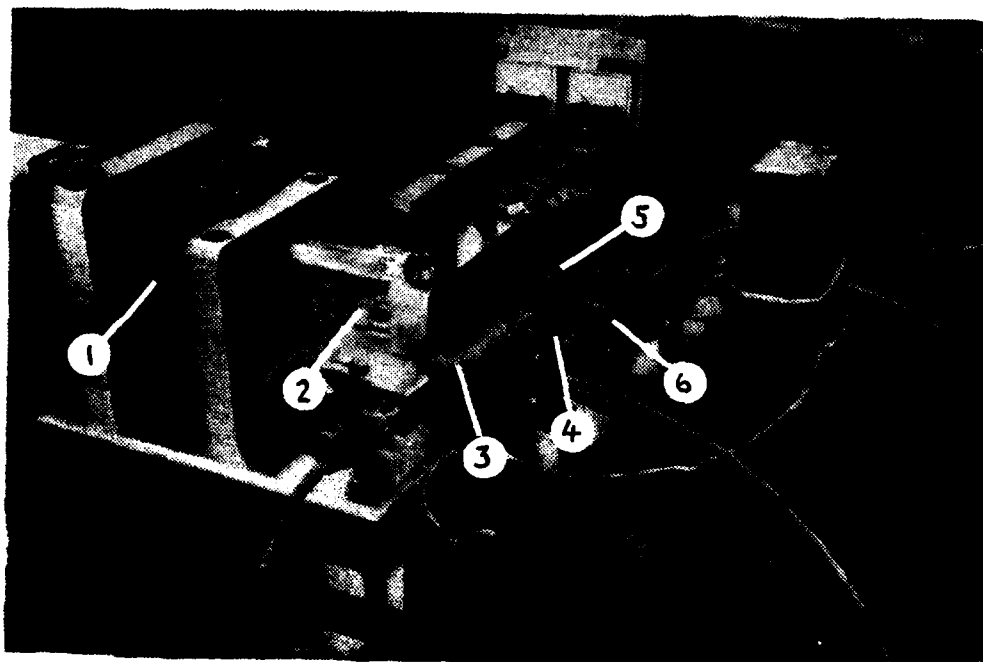
Items indicated are: (1) electric motor, (2) plexiglas cavity, (3) light-
sensitive diode, (4) proximity sensor, (5) solenoid-actuated plunger, (6)
air-jet nozzle.

Figure 9: Photograph of Spin-up Rig
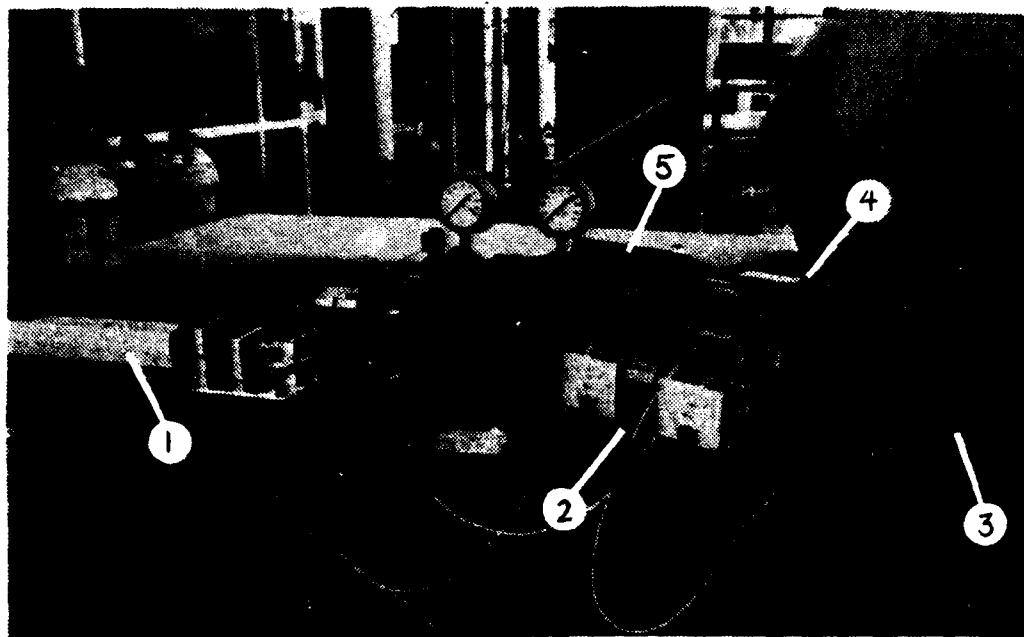
Items indicated are: (1) laser, (2) electrical motor power supply, (3) proximity-sensor amplifier, (4) timer, (5) counter.

Figure 10: Photograph of Spin-up Rig with Instrumentation

2. Mechanical Holding Device

In spite of the improved seating arrangement for the ball when under the influence of the holding jet, slippage continued to occur at high spin rates. This necessitated another modification to the apparatus. The holding jet was replaced with the mechanical holding device illustrated in the following schematic (Fig. 11). The plunger has a guide which is attached to the rotating cylinder, hence it is free to move only in the axial direction. Four small notches were bored into the exterior of the ball to accommodate the prongs on the plunger portion of this holding device. The ball is held in place in its initial position by placing a weight on the pendulum portion of the mechanism. After
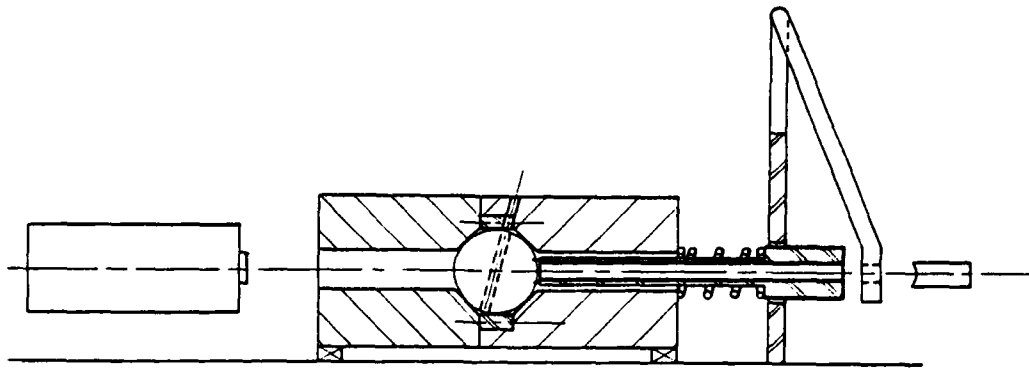
Ball in initial position showing pronged plunger, plunger spring, holding pendulum.

Figure 11:   Schematic of Mechanical Holding Device

a desired speed of rotation is achieved, the weight is removed and the plunger is pushed away from the ball by the mechanism's spring. At the instant the ball is free from the plunger, a magnetic band on the plunger passes by a magnetic sensitive diode and an electric timer is started. After the ball nutates through a large enough angle $(\theta_0 - \theta^*)$, the laser beam becomes unobstructed and passes through the hollow plunger directly into a light-sensitive diode, stopping the timer, and ending the event. Figure 12 is a photograph of the apparatus with this holding device.
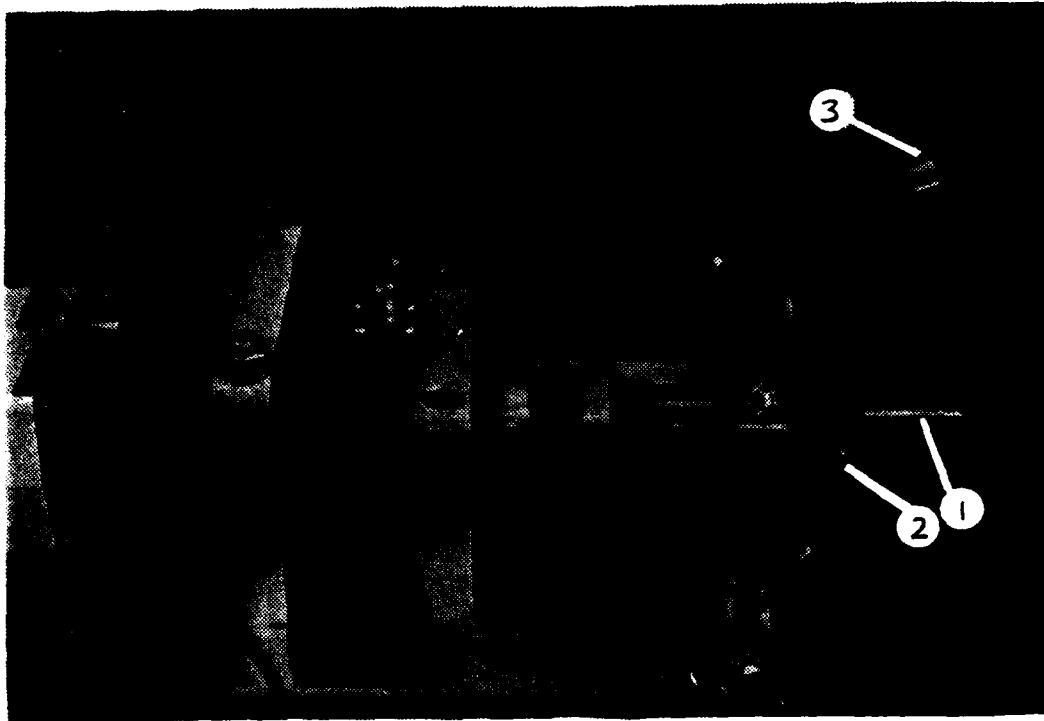
Items indicated are: (1) plunger, (2) proximity sensor, (3) holding pendulum.

Figure 12: Photograph of Spin-up Rig with Mechanical Holding Device

III. DISCUSSION OF RESULTS

A. AIR JET HOLDING DEVICE

1. Steel on Plexiglas

Table I of Appendix A represents the experimentally determined elapsed times t* required for: Ball 1 to nutate through a set increment, $\theta_0 - \theta^*$, at various spin rates, ω_0. Figure 13 is the graphical representation of these data and illustrates that for large ω_0, the data agrees with a curve of the form:

$$t^* = T\,\omega_0 + b$$

where b is the t* intercept

From Eq. (8)

$$T = \frac{\pi A\left[(\theta_0 - \theta^*) - \frac{\lambda}{2}\sin 2\,\theta_0\right]}{2_{u_s}\,WR\,\sin\theta_0\,E\,(\theta_0)}$$

where A, θ_0, θ^*, λ, W, and R are given in Appendix A.
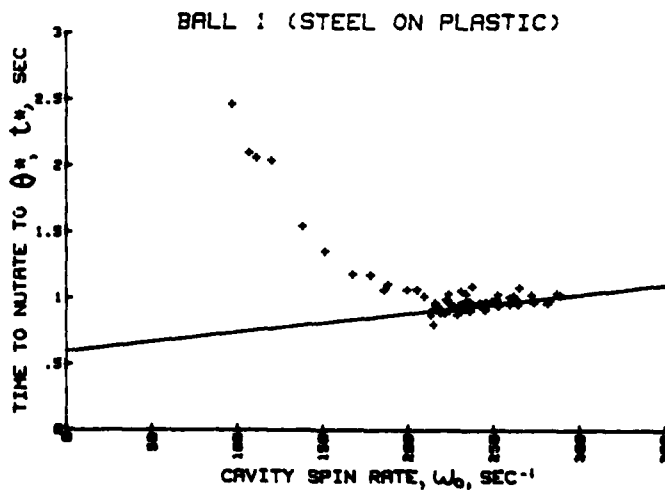
Figure 13: Graph of t* v.s. ω_0 for Steel on Plexiglas, Ball 1.

Using the published coefficient of friction between steel and laminated plastic of $\mu_s = .35$ [6] and solving Eqs. (9)-(10) yields a minimum spin rate of 214 rad/sec necessary for the linear response. It is necessary to get spin rates substantially higher than this minimum value if a linear relationship between t* and ω_0 is to be assured. Because of the holding jet's inability to hold the ball in position at spin rates greater than 289 rad/sec, however, the data in Table I and Fig. 13 are marginally acceptable for analysis.

The following discussion illustrates this problem. For Ball 1 at large ω_0 (Appendix A):

$$t^* = \frac{.842 \times 10^{-3} \ sec^2}{\mu_s} \omega_0 + b$$

A least squares fit to the data of the line $t^* = T\omega_0 + b$ gives the most probable value of T over the range of the data used. The following table illustrates the dependency of T on this range:

$$\omega_0 \geq 220 \ rad/sec, \quad T_{220} = 9.481 \times 10^{-4} \ sec^2$$

$$\omega_0 \geq 240 \ rad/sec, \quad T_{240} = 1.310 \times 10^{-3} \ sec^2$$

$$\omega_0 \geq 270 \ rad/sec, \quad T_{270} = 1.445 \times 10^{-3} \ sec^2$$

and solving for $\mu_s = \frac{.842 \times 10^{-3} \ sec^2}{T}$ yields:

$$(\mu_s)_{220} = 0.89$$

$$(\mu_s)_{240} = 0.64$$

$$(\mu_s)_{270} = 0.58$$

The best approximation is calculated from the highest spin rates and gives μ_s = .58. This value is high compared to the previously mentioned published value of .35. It appears, however, that if higher spin rates could have been achieved, a lower value for μ_s would have been determined.

Experimentation with this apparatus was also limited in precision because of the interaction between the holding jet and the solenoid-actuated plunger. The speed of retraction of the plunger varied by as much as 0.005 sec. Also, the rotation of the spin-up rig would vary by as much as 1 rad/sec, and the initial position of the ball varied by up to 2 degrees. All of these discrepancies affect t* and contribute to the scatter of data.

The variance for T is given by:

$$\sigma_T^2 = \frac{N\sigma^2}{N \sum\limits_{i=1}^{N} \omega_{o_i}^2 - \left(\sum\limits_{i=1}^{N} \omega_{o_i} \right)^2}$$

where

$$\sigma^2 = \frac{1}{N} \sum\limits_{i=1}^{N} (T\omega_{o_i} + b - t_i^*)^2$$

Evaluating the standard deviation yields $(\sigma_T)_{270} = 1.749 \times 10^{-3}$ sec, and

$$\frac{(\sigma_T)_{270}}{T_{270}} = 1.21$$

so the percent standard deviation for T_{270} is 121%. That is, there is a 68% statistical probability that the true value lies within 1.21 standard deviations of the least squares value.

B. MECHANICAL HOLDING DEVICE

1. Ball 2 ($\hat{r} = 0.2$)

Ball 2 was essentially identical to Ball 1 except for the small notches required to accommodate the mechanical holding device. In the series of tests using this ball, however, the cylinder insert sleeves were used to evaluate the performance of the system for the cases of steel-on-steel and steel-on-aluminum.

Tables II and III of Appendix B represent the experimentally determined time t^* required for Ball 2 to nutate through a set increment, $\theta_0 - \theta^*$, at various spin rates, with steel and aluminum inserts respectively. Figures 14 and 15 are the graphical representation of these data.
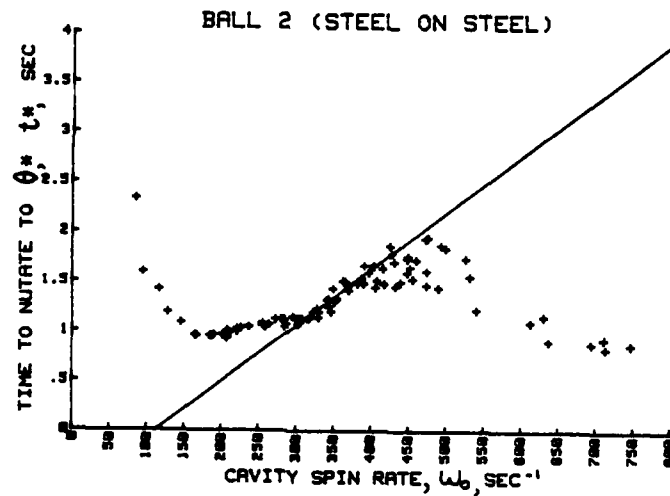
Figure 14: Graph of t^* v.s. ω_0 for Steel on Steel, Ball 2.

30

Figure 15: Graph of t* v.s. ω_0 for Steel on Aluminum, Ball 2.

The following discussion pertains to both figures but will be limited in specifics to Fig. 14. (Figure 15 illustrates the similarity of results regardless of materials used.) As ω_0 gets large, the data appears to asymptotically approach a curve of the form

$$t^* = T\omega_0 + b$$

but at spin rates greater than about 380 rad/sec the data starts to scatter radically and t* starts to drop off. Using the published co-efficient of friction [6], $0.42 < \mu_s < 0.57$, between steel and steel and solving Eqs. (9)-(10) yields a minimum spin rate of 272 rad/sec necessary for the linear response to apply. A least squares fit to the data of the line $t^* = T\omega_0 + b$ for 300 rad/sec $< \omega_0 < 382$ rad/sec yields:

$$T = 5.672 \times 10^{-3} \text{ sec}^2$$

31

and

$$\mu_s = \frac{.844 \times 10^{-3} \text{ sec}^2}{T} = 0.15$$

This apparent poor agreement with the published value may be due to several factors. First, the range of values used for ω_0 is not much greater than the minimum required spin rate of 272 rad/sec. Secondly, because of the relatively small value of $\hat{r} = 0.2$, the inertial imbalance of the ball is small and t^* is relatively large. The inertial characeristics of the motion are therefore easily influenced by uncontrollable experimental uncertainties and it is thought that this contributed significantly to the scatter of data. Thirdly, because of the as-yet unexplained high-speed fall-off, comparison of the linear approximation with the exact solution isn't as favorable for large t^* as for small t^*. And finally, the ratio of the volume of material removed from the ball's surface to accommodate the prongs of the holding mechanism to the volume removed to bore the ball's concentric hole is about 1 to 10 which may be large enough to affect ball motion.

The reason for the scatter of data and reduced times for nutation when $\omega_0 > 380$ rad/sec is unknown. One possible cause is that the drag between the plunger and its guide may be significant enough at these spin rates to reduce its speed of retraction thus delaying the start of the electric timer and artifically reducing the recorded value of the elapsed time. Also, this may be the range of spin rates where the inertial imbalance forces begin to overcome any initial delaying effects due to static friction. This would account for the severe scatter of data for spin rates in the range of 400-500 rad/sec followed by reduced scatter and lower elapsed times at higher spin rates.

32

2. __Ball 3 ($\hat{r} = 0.5$)__

Tables IV and V of Appendix C represent the experimentally de-
termined time t* that it took Ball 3 to nutate through a set increment,
$\theta_0 - \theta*$, at various spin rates, with steel and aluminum inserts respectively.
Figures 16 and 17 are the graphical representation of these data.

BALL 3 (STEEL ON STEEL)
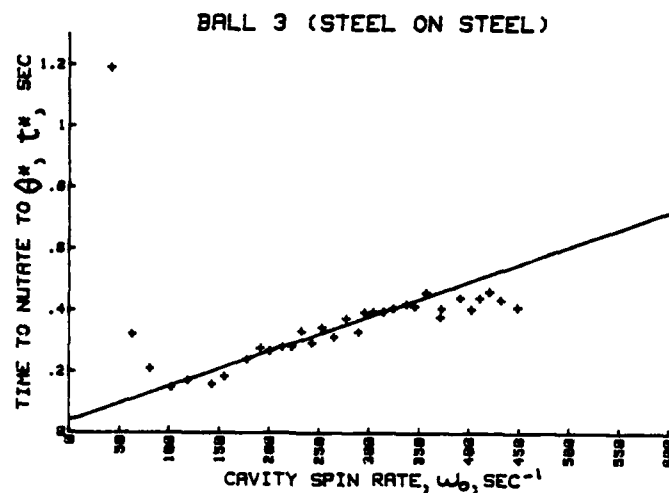
Figure 16: Graph of t* v.s. ω_0 for Steel on Steel, Ball 3.
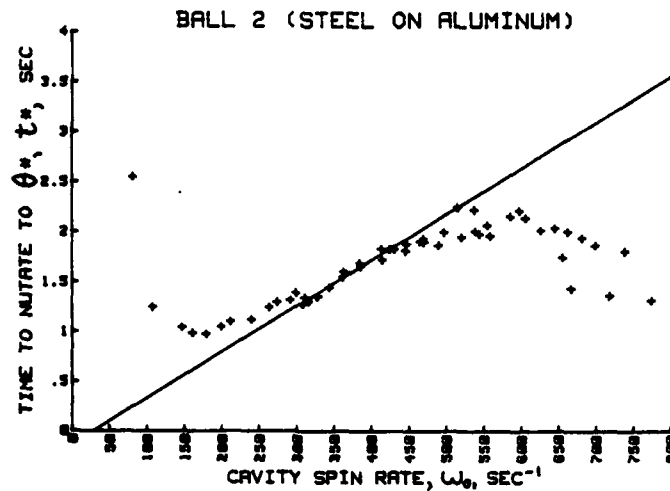
BALL 3 (STEEL ON ALUMINUM)
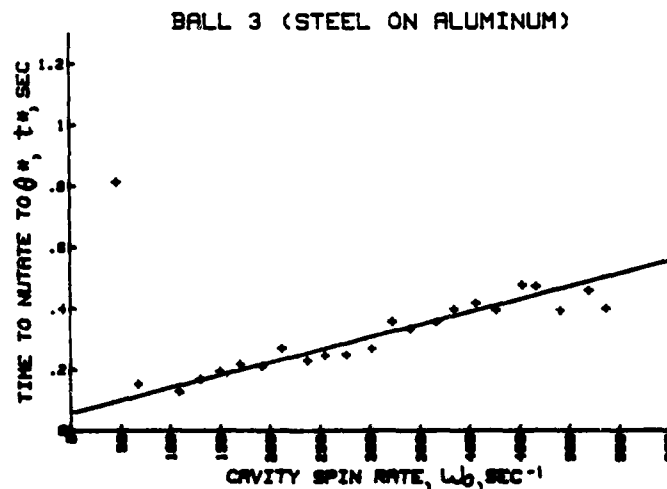
Figure 17: Graph of t* v.s. ω_0 for Steel on Aluminum, Ball 3.

33

As before, this discussion pertains to both figures but will be limited in specifics to Fig. 16. Figure 17 is present to reconfirm the nature of the results regardless of materials used. As ω_0 gets large the data approach a curve of the form

$$t^* = T\omega_0 + b$$

but then, at about 350 rad/sec the data scatter increases and t^* shows a tendency to drop off. Solving Eqs. (9)-(10) yields a minimum spin rate of 120 rad/sec necessary for the linear response to apply. A least squares fit of this line to the data for 200 rad/sec $<\omega_0<$ 320 rad/sec yields

$$T = 1.138 \times 10^{-3} \text{ sec}^2$$

and

$$\mu_s = \frac{.598 \times 10^{-3} \text{ sec}^2}{T} = 0.52$$

with a standard deviation of 1.5×10^{-4} sec^2 and a percent standard deviation of 13.6%. That means that there is a 95% probability that the true value lies within .272 standard deviations of the least squares value. The experimental uncertainties associated with this formula are given in Appendix D. The overall uncertainty in μ_s is estimated to be about 13.4%. The largest contribution to this uncertainty is due to the estimated uncertainty in θ_0.

This good agreement with the published value can be attributed to several factors. First, the range of spin rates used is approximately two to three times the minimum spin rate of 120 rad/sec, making this data better for analysis than the data obtained with Ball 1 and Ball 2 ($\hat{r} = 0.2$). Secondly, because of the relatively large hole in Ball 3 ($\hat{r} = 0.5$), the

34

inertial imbalance is large and t* is small, with less tendency for error accumulation during this event. Thirdly, comparison of the linear approximation with the exact solution is more favorable for small t* than for large t*. Finally, with the larger hole the effect of material removed from the ball to accommodate the prongs of the holding device should have little if any effect on ball motion.

The reasons for the reduced times of nutation at high spin rates are thought to be the same as those described in the discussion of Ball 2. These effects begin to occur at somewhat lower spin rates because Ball 3 has a greater inertial imbalance than Ball 2. As a matter of fact, the forces on the holding mechanism were so great at higher spin rates that the actuator spring force was insufficient to overcome them and retract the plunger. For this reason, experimentation was limited to spin rates less than 450 rad/sec. It is felt that if higher spin rates could have been achieved, correspondingly larger values of t* would have been measured.

IV. CONCLUSION AND RECOMMENDATIONS

Recalling that the purpose of this study has been to determine if the friction-driven gyroscopic mass, and the associated experimental apparatus is a feasible means for the determination of the coefficient of sliding friction, it is not possible at this time to provide a definitive answer. The basic trends predicted by the theoretical model were observed in all cases, but these trends were often obscured by difficulties with the test apparatus. However, significant confidence in the approximation and methods used was gained, especially after reviewing the data for Ball 3.

It is felt more testing is required; specific recommendations are:

(1) More experimentation should be performed to see what affects $\hat{r}$ has on t*. Theoretically the maximum value of $\hat{r}$ is unity, but it is felt too large a hole could cause the ball to get stuck in the cylinder cavity.

(2) The minimum number of prongs needed on the plunger of the mechanical holding device to hold the ball in its initial position should be experimentally determined.

(3) An insert with a known coefficient of sliding friction between it and the ball should be used to determine if calibration is necessary.

(4) A more direct (possibly optical) method of determining the actual start of ball nutation is needed. Presently, an electric timer is started when a metal band on the plunger passes by a proximity sensor. Because the plunger motion can be erratic, this starting time may be a significant source of uncertainty.

36

(5) If the present design is retained, a stronger spring or a different (possibly solenoid-actuated) method of retracting the plunger is needed so that higher spin rates and repeatable starting times can be achieved.

(6) Testing of different materials should be conducted.

APPENDIX A

Design Calculations and Experimental Results for Ball 1

I. Ball Dimensions
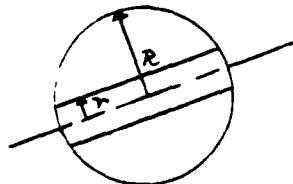
$r = 0.0936$ inches
$R = 0.4682$ inches
$W = 51.755$ grams $= .1141$ lbs
$\theta_0 = 77°$
$\rho = 487.87$ lb/ft^3

II. Calculations [1]

$E(\theta_0) = 1.0611$ [7]

$\hat{r} = \dfrac{r}{R} = .1999$

$\lambda = \dfrac{5\hat{r}^2}{\hat{r}^2+4} = .049484$

$\theta^* = \sin^{-1}\hat{r} = 11.534°$

$A = \dfrac{4\pi\rho R^5}{15g_c}\left[.5(1-\hat{r}^2)^{1.5}(3\hat{r}^2+2)+(1-\hat{r}^2)^{2.5}\right] = 2.180 \times 10^{-6}$ ft·lb·sec^2

$M = \dfrac{2\mu_s WR(\lambda+1)E(\theta_0)}{\pi\lambda A\omega_0^2\cos\theta_0} = 1.300 \times 10^5$ sec^{-2} $\dfrac{\mu_s}{\omega_0^2}$

$\zeta = \dfrac{M}{2} = 6.500 \times 10^5$ sec^{-2} $\dfrac{\mu_s}{\omega_0^2}$

Eq. (9) $\omega_0 \geq \sqrt{\dfrac{4\mu_s WRE(\theta_0)}{\pi A\lambda\sin2\theta_0}} = 356.59\sqrt{\mu_s}$ rad/sec

Eq. (10) $\omega_0 \gg \sqrt{\dfrac{2\mu_s WR(\lambda+1)E(\theta_0)}{\pi\lambda A\cos\theta_0}} = 360.6\sqrt{\mu_s}$ rad/sec

$$t^* = \frac{\pi A\omega_0\left[(\theta_0-\theta^*)-\dfrac{\lambda}{2}\sin2\theta_0\right]}{2\mu_s WR\sin\theta_0 E(\theta_0)} = \frac{.842 \times 10^{-3} \sec^2 \omega_0}{\mu_s}$$

$$\mu_s = \frac{.842 \times 10^{-3} \sec^2 \omega_0}{t^*}$$

39

Table 1

Tabulated Results for Ball 1 on Plastic

#	$\omega_0 (sec^{-1})$	t*(sec)	#	$\omega_0 (sec^{-1})$	t*(sec)
1	63.5	3.524	2	96.8	2.465
3	106.8	2.100	4	111.0	2.060
5	119.8	2.041	6	138.2	1.545
7	151.2	1.356	8	167.6	1.184
9	178.0	1.178	10	185.6	1.064
11	188.1	1.107	12	199.2	1.064
13	205.2	1.070	14	209.2	1.017
15	213.2	.874	16	214.3	.922
17	214.7	.803	18	215.3	.949
19	216.8	.922	20	215.5	.967
21	219.1	.891	22	217.4	.938
23**	221.8	.994	24**	221.6	.891
25**	223.0	.988	26**	220.0	.992
27**	224.1	.913	28**	223.5	1.036
29**	226.6	.943	30**	224.7	.954
31**	228.7	.877	32	228.7	.915
33**	230.8	.936	34	230.4	.918
35**	231.0	.916	36	230.8	1.059
37**	232.9	.984	38	231.2	.968
39**	233.3	.957	40	233.1	.925
41**	233.7	.965	42	233.7	1.035
43	215.3	.969	44	234.6	.955
45**	235.2	.970	46	235.8	.974
47**	236.0	.976	48	236.2	.906
49**	237.3	1.093	50	237.5	.950
51**	241.5	.966	52	241.9	.957
53**	244.0	.926	54	245.0	.916
55**	245.3	.976	56	245.7	.956
57**	248.8	.978	58	248.8	.972
59	251.3	.999	60	251.7	.989
61	252.2	.959	62	252.2	1.032
63	252.6	.945	64	258.9	.958
65	259.1	1.011	66	261.4	1.026
67	263.1	.998	68	263.9	.978
69	263.9	.958	70	264.7	1.086
71**	271.8	1.030	72**	273.3	.971
73**	281.3	.963	74**	282.7	.987
75**	286.7	1.037	76**	288.6	1.028

** Used for least squares fit.

APPENDIX B

Design Calculations and Experimental Results for Ball 2

I. Ball Dimensions
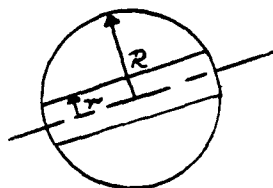
r = 0.0935 inches
R = 0.4682 inches
W = 51.613 grams = .1138 lbs
θ_0 = 77°
ρ = 487.87 lb/ft³

II. Calculations (See Appendix A for formulas)

$E(\theta_0) = 1.0611$

$\hat{r} = .1997$

$\lambda = .0493689$

$\theta^* = 11.521°$

$A = 2.18 \times 10^{-6}$ ft·lb·sec²

$M = 1.300 \times 10^5$ sec^{-2} $\dfrac{\mu_s}{\omega_0^2}$

$\zeta = 6.500 \times 10^5$ sec^{-2} $\dfrac{\mu_s}{\omega_0^2}$

Eq. (9) $\omega_0 \geq 356.6 \sqrt{\mu_s}$ rad/sec

Eq. (10) $\omega_0 \gg 360.6 \sqrt{\mu_s}$ rad/sec

$$\mu_s = \frac{.844 \times 10^{-3} \text{ sec}^2 \, \omega_0}{t^*}$$

41

Table II

Tabulated Results for Ball 2 on Steel

#	$\omega_0 (\text{sec}^{-1})$	t*(sec)	#	$\omega_0 (\text{sec}^{-1})$	t*(sec)
1	116.45	1.4236	2	747.28	.8767
3	145.56	1.0884	4	285.68	1.0799
5	165.88	0.9555	6**	301.80	1.0741
7	189.54	0.9628	8**	304.53	1.0953
9	207.97	0.9235	10**	329.03	1.1446
11	211.74	0.9890	12**	329.66	1.1946
13	226.82	1.0361	14**	346.41	1.2038
15	263.47	1.0730	16**	353.95	1.3323
17	271.85	1.1253	18**	369.24	1.4557
19	295.31	1.1510	20	386.83	1.5435
21**	315.21	1.1312	22	390.19	1.4874
23**	342.64	1.3293	24	405.89	1.4472
25**	351.02	1.3023	26	407.99	1.5164
27**	362.33	1.5122	28	432.70	1.4555
29**	381.81	1.4857	30	439.19	1.5005
31	403.59	1.6638	32	449.46	1.7618
33	425.58	1.8617	34	454.90	1.5303
35	448.20	1.7338	36	473.75	1.6096
37	459.72	1.7225	38	473.33	1.4690
39	489.67	1.4425	40	540.14	1.2210
41	531.77	1.5546	42	637.53	0.9115
43	630.41	1.1569	44	713.56	0.8386
45	711.26	0.9369	46	95.29	1.5971
47	84.82	2.3362	48	127.97	1.1922
49	186.61	0.9542	50	163.78	0.9641
51	220.96	1.0312	52	183.89	0.9559
53	201.90	0.9655	54	207.97	1.0104
55	254.68	1.0871	56	221.38	.9995
57	258.66	1.0395	58	236.88	1.0475
59	283.79	1.0442	60	254.68	1.0640
61	283.58	1.1246	62	396.89	1.5960
63	279.81	1.1232	64	390.60	1.6655
65	299.29	1.1335	66	415.74	1.6374
67**	302.64	1.1283	68	417.62	1.4831
69**	306.83	1.1333	70	431.03	1.7030
71**	316.67	1.1371	72	427.88	1.7863
73**	321.70	1.1996	74	447.78	1.5947
75**	327.56	1.2365	76	451.55	1.6480
77**	343.48	1.2526	78	475.22	1.9419
79**	340.34	1.3181	80	472.29	1.9333
81**	348.93	1.4350	82	493.44	1.8681
83**	365.68	1.5002	84	499.51	1.8374
85**	365.25	1.5048	86	526.53	1.7356
87**	370.08	1.4176	88	612.40	1.0982
89	387.67	1.5309	90	694.92	.8886

** Used for least squares fit.

42

Table III

Tabulated Results for Ball 2 on Aluminum

#	$\omega_0 (\text{sec}^{-1})$	$t^*(\text{sec})$	#	$\omega_0 (\text{sec}^{-1})$	$t^*(\text{sec})$
1	263.47	1.2405	2**	315.83	1.2993
3	273.74	1.2939	4**	327.77	1.3480
5	298.03	1.3866	6**	343.06	1.4390
7**	362.33	1.6002	8**	360.86	1.5459
9**	385.37	1.6528	10**	383.90	1.6864
11**	413.22	1.8298	12**	414.48	1.7167
13**	430.40	1.8274	14**	424.74	1.8275
15	446.32	1.8753	16	445.27	1.8086
17	464.33	1.9031	18	468.52	1.9297
19	496.37	1.9948	20	469.56	1.8941
21	514.80	2.2455	22	489.46	1.8633
23	537.00	2.2207	24	519.83	1.9481
25	553.76	2.0643	26	537.84	2.0068
27	596.90	2.2128	28	543.08	1.9757
29	655.34	1.7427	30	557.53	1.9590
31	717.33	1.3615	32	584.55	2.1527
33	773.67	1.3147	34	605.49	2.1385
35	211.74	1.0990	36	625.81	2.0150
37	80.84	2.5442	38	644.86	2.0357
39	107.65	1.2430	40	666.23	1.4305
41	146.40	1.0385	42	662.04	2.0013
43	160.43	0.9831	44	680.68	1.9390
45	178.65	0.9709	46	698.48	1.8664
47	198.97	1.0431	48	738.27	1.8066
49	239.60	1.1144	50	291.12	1.3132
51**	310.18	1.3404	52**	308.29	1.2727

** Used for least squares fit.

APPENDIX C

Design Calculations and Experimental Results for Ball 3

I. **Ball Dimensions**
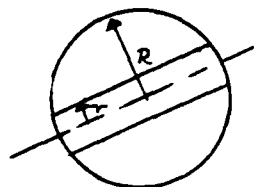
$r = 0.2344$ inches
$R = 0.4682$ inches
$W = 35.2764$ grams $= .0778$ lbs
$\theta_0 = 77°$
$\rho = 487.87$ lb/ft^3

II. **Calculations (See Appendix A for formulas)**

$E(\theta_0) = 1.0611$

$\hat{r} = .5006$

$\lambda = .2948275$

$\theta^* = 30.042°$

$A = 1.584 \times 10^{-6}$ ft·lb·sec^2

$M = 2.527 \times 10^4$ sec^{-2} $\dfrac{\mu_s}{\omega_0^2}$

$\zeta = 1.263 \times 10^4$ sec^{-2} $\dfrac{\mu_s}{\omega_0^2}$

Eq. (9) $\quad \omega_0 \geq 141.5 \sqrt{\mu_s}$ rad/sec

Eq. (10) $\quad \omega_0 \gg 159.0 \sqrt{\mu_s}$ rad/sec

$$\mu_s = \frac{.598 \times 10^{-3} \text{ sec}^2 \, \omega_0}{t^*}$$

44

Table IV

Tabulated Results for Ball 3 on Steel

#	$\omega_0 (\text{sec}^{-1})$	$t^*(\text{sec})$	#	$\omega_0 (\text{sec}^{-1})$	$t^*(\text{sec})$
1	41.26	1.1908	2	391.44	.4422
3	62.41	.3231	4	410.92	.4410
5	80.63	.2105	6	432.07	.4343
7	101.79	.1483	8	448.62	.4114
9	118.33	.1728	10	370.92	.3792
11	142.21	.1590	12**	191.64	.2766
13	154.99	.1842	14**	213.42	.2824
15	178.02	.2399	16**	232.06	.3312
17**	201.27	.2681	18**	252.58	.3449
19**	222.84	.2837	20**	277.09	.3740
21**	242.32	.2950	22	295.75	.3945
23**	264.52	.3143	24	314.58	.3972
25**	289.03	.3308	26	337.41	.4227
27**	304.73	.3954	28	356.47	.4594
29**	324.68	.4080	30	402.54	.4048
31	345.58	.4146	32	420.35	.4615
33	372.17	.4072			

** Used for least squares fit.

45

Table V

Tabulated Results for Ball 3 on Aluminum

#	$\omega_0 (\text{sec}^{-1})$	t*(sec)	#	$\omega_0 (\text{sec}^{-1})$	t*(sec)
1	108.91	.1277	2**	366.31	.3568
3**	129.85	.1701	4**	383.90	.3988
5**	149.12	.1945	6**	405.89	.4182
7**	169.65	.2189	8	426.00	.3950
9**	191.64	.2122	10	452.39	.4786
11**	211.32	.2706	12	466.21	.4735
13**	236.67	.2301	14	490.09	.3936
15**	254.47	.2460	16	519.20	.4593
17**	276.04	.2491	18	536.17	.3993
19**	301.80	.2686	20	67.44	.1531
21**	322.33	.3570	22	45.87	.8146
23**	340.13	.3347			

** Used for least squares fit.

46

APPENDIX D

Uncertainty Analysis for Ball 3, Steel on Steel

I. Point of Evaluation

$\theta_0 = 77°$ $A = 1.584 \times 10^{-6}$ ft·lb·sec^2

$\theta^* = 30°$ $W = 0.0778$ lbs

$\hat{r} = 0.5$ $R = 0.4682$ inches

$\lambda = 0.295$ $E(\theta_0) = 1.0611$

II. Calculations (assuming $\Delta A = \Delta \lambda = \Delta W = \Delta R = \Delta E(\theta_0) = 0$)

$$\mu_s = \left[\frac{\pi A \left[(\theta_0 - \theta^*) - \frac{\lambda}{2} \sin 2\theta_0 \right]}{2WR \sin\theta_0 E(\theta_0)} \right] \frac{\omega_0}{t^*}$$

so

$$\frac{\Delta \mu_s}{\mu_s} = \left[\left(\frac{\Delta k}{k} \right)^2 + \left(\frac{\Delta \omega_0}{\omega_0} \right)^2 + \left(\frac{\Delta t^*}{t^*} \right)^2 \right]^{1/2}$$

where

$$k = \frac{\pi A \left[(\theta_0 - \theta^*) - \frac{\lambda}{2} \sin 2\theta_0 \right]}{2WR \sin\theta_0 E(\theta_0)} = \frac{k_1 \left[(\theta_0 - \theta^*) - k_2 \sin 2\theta_0 \right]}{\sin\theta_0}$$

$$\frac{\Delta k}{k} = \frac{1}{k} \left[\frac{\partial k \Delta \theta_0}{\partial \theta_0} + \frac{\partial k \Delta \theta^*}{\partial \theta^*} \right]$$

assuming $\Delta \theta_0 = 5°$ and $\Delta \theta^* = 2°$ and substituting

σ_T^2 (evaluated on pg. 33) in place of $\left(\frac{\Delta \omega_0}{\omega_0} \right)^2 + \left(\frac{\Delta t^*}{t^*} \right)^2$

yields

$$\frac{\Delta \mu_s}{\mu_s} = .134 \text{ or } 13.4\%$$

47

LIST OF REFERENCES

1. Nunn, R. H., and Bloomer, J. W. II, "Motion of a Bored Sphere in a Spinning Spherical Cavity", J. Dynamic Systems, Measurement and Control, v. 103, No. 4, pp. 389-394, Dec. 1981.

2. Nunn, R. H., and Bloomer, J. W. II, "Ball-Obturation of a Spinning Tubular Projectile", J. Spacecraft and Rockets, v. 18, No. 6, pp. 533-539, Nov.-Dec. 1981.

3. Naval Postgraduate School Report No. 69-81-001, Ball Motion in a Ball-Obturated Tubular Projectile, by Nunn, R. H., and Bloomer, J. W. III, Jan. 1981.

4. Rabinowicz, Earnest, Friction and Wear of Materials, pp. 95-99, Wiley, 1965.

5. Bowden and Tabor, The Friction and Lubrication of Solids, Pt. II, pp. 452-456, Oxford, 1964.

6. Marks, L. S., Standard Handbook for Mechanical Engineering, 8th ed., pp. 3.24-3.27, McGraw Hill, 1979.

7. C.R.C. Standard Mathematical Tables, 12th Ed., pp. 257-259, Chemical Rubber, 1959.

INITIAL DISTRIBUTION LIST

		No. Copies
1.	Defense Technical Information Center Cameron Station Alexandria, Virginia 22314	2
2.	Library, Code 0142 Naval Postgraduate School Monterey, California 93940	2
3.	Department Chairman, Code 69Mx Department of Mechanical Engineering Naval Postgraduate School Monterey, California 93940	2
4.	Professor R. H. Nunn, Code 69Nn Naval Postgraduate School Monterey, California 93940	5
5.	LT. Thomas L. Stowell Rt. 3, Box 472B Florence, South Carolina 29501	1

ME8